CEDTECH International Journal of Engineering & Applied Science
Volume 2, Number 4, December 2021
http://www.cedtechjournals.org
ISSN: 2756-4533

APPLICATION OF COMPUTATIONAL FLUID DYNAMICS SOFTWARE IN THE FORMATION AND DISSOCIATION OF HYDRATES IN PIPELINES

Oluwafemi Olayebi
Department of Chemical Engineering
Federal University of Petroleum Resources, Delta State, Nigeria
Email: olayebi.oluwafemi@fupre.edu.ng

ABSTRACT

Gas hydrates have been identified as obstacles in the gas industry in which under certain temperature and pressure conditions, a lattice of water surrounds gas molecules such as methane, ethane, or carbon dioxide and generates a stable solid, similar to ice water. This work aims to review the formation and dissociation of hydrates, evaluate the equations governing them and apply CFD software to hydrate formation and dissociation in pipelines. Steel pipeline was considered and the fluid flow was taken as incompressible using SIMSCALE software. At low temperature and high pressure, hydrates tend to form in pipelines. Length, time, mass flow rate were parameters used to predict hydrate formation in pipelines. Introduction of inhibitors were found to reduce or eliminate hydrate formation.

INTRODUCTION

Gas hydrates are ice-like crystalline compounds formed by 3-dimensional hydrogen-bonded water lattices that trap small gas molecules. The water molecules are usually referred to as host molecules, while the gas molecules as guest molecules. Chemical bonds are not known to be established between the hydrocarbon and water molecules which are known to form a cage through the hydrogen bonds. The small gas molecules trapped inside this cage are free to rotate within the void space. With

respect to natural gas, hydrate formation in pipelines undermines flow assurance programs posing a threat to personnel and equipment, blocking the pipelines and becoming obstacles in the gas industry (Gong and Lv, 2013). Under certain temperature and pressure conditions, a lattice of water surrounds the gas molecules which can be methane, ethane etc, and generate a stable solid that is similar to ice water. Gas hydrates can form at atmospheric pressure and at about -20^{o}C (Chen *et al.*, 2018) and the blockages formed appear like ice water (Merey and Longinos, 2018) although they can also form well above the freezing point of water at high pressures. Also, non-stoichiometric mixtures of water and natural gas form Clathrate hydrates in which the gas molecules are trapped in a polygonal crystalline structure made of water molecules (Jai et. al, 2020). The water molecules arrange themselves in an orderly fashion around the gas molecules, thus entrapping them. Essentially, the requirements for hydrate formation include low temperature, high pressure, with the stream of natural gas or light hydrocarbons in the presence of water (Seyyedbagheri and Mirzayi, 2016). Hence, the elimination of one of these three factors is essential for eliminating and controlling hydrate formation in pipelines.

Hydrate Formation Process

The formation of hydrate involves two distinct processes which are nucleation and crystal growth and which are time-dependent (Liu, 2017). Hydrate nucleation process involves small clusters of water and gas growing to a critical size and in which water molecules cluster around the dissolved gas molecules. The nucleus with a critical radius is in equilibrium with the

surrounding medium. With regard to this, Seyyedbagheri and Mirzayi (2016) have opined that nucleation has an advantage with respect to natural gas storage while the crystal growth process is thought to have an advantage in terms of production and transportation of oil and gas. The knowledge of the dynamics of hydrate formation and accumulation of hydrate crystals is important in determining the parameters for mass production of gas hydrates, and in understanding plug conditions in the gas pipeline. Mamasani *et al.*, (2019) have also mentioned that the sequence of events leading to hydrate formation in gas pipelines involves water vapor condensation, water accumulation at lower sections of pipelines, nucleation, and growth of hydrate particles which ultimately block the pipeline. The site of hydrate deposition may not be the same as that in which the pipeline blockage occurs because at the beginning of summer, hydrates are released from the pipeline walls along the pipe length and may migrate downstream and eventually deposit at the sagging sections of the pipeline leading to blockage (Nik, 2021). With respect to natural gas, the pictorial view of the lattice structure of gas hydrate is shown in Figure 1. Methane gas is the guest in the middle (Green) while water molecule is the host (Red).

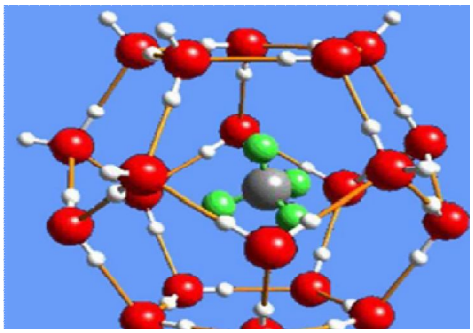

Figure 1: Gas hydrate surrounded by a water molecule (Shi *et al.*, 2016)

As oil/gas subsea fields mature, the amount of water produced increases significantly as a result of the production methods employed for the enhancement of oil recovery. This is especially true in the case of oil reservoirs (Majlesara et. al., 2013).

Properties of Hydrates

It is generally possible to remove the water of hydration by heating the hydrate. The residue obtained after heating, called the anhydrous compound, will have a different structure and texture and may have a different colour than the hydrate (Shi *et al.*, 2018). An example is shown in the following equations:

$CuSO_4 \cdot 5H_2O(s)$ (Deep Blue) $\rightarrow \Delta CuSO_4(s)$ (Ashy White) $+5H_2O(g)$

$CuSO_4(s)$ (Ashy White) $\rightarrow H_2O(l).CuSO_4(aq)$ (Deep Blue)

Any anhydrous compound from a hydrate generally has the following properties:

1. They are highly soluble in water
2. When dissolved in water, the anhydrous compound will have a color similar to that of the original hydrate, even if it had changed color when transiting from the hydrate to the anhydrous compound.

Most hydrates are stable at room temperature. However, some are efflorescent and spontaneously lose water upon standing in the atmosphere. Some other compounds release water upon heating by decomposition of the compound rather than by losing their water of hydration. An example of this are carbohydrates which are not considered true hydrates because the hydration process is not reversible (Mamasani *et al.*, 2019).

Hydrate formation

A mathematical model proposed to study hydrate formation reported that sudden pressure drop on either side of the hydrated mass causes its phase to be frozen, and the reduction of high pressure leads to increase in the drying time of the ice mass relative to the hydrate (Seyyedbagheri and Mirzayi, 2017).

In practical terms, the present hydrate risk management strategy is to allow transportable hydrates to form in pipelines than to prevent hydrate formation completely (Yao *et al.*, 2019) and in this case, it is advisable to consider a comprehensive hydrate formation and transportability model which would incorporate hydrate formation and plugging mechanisms in various scenarios of oil and gas production and in which oil is the continuous phase and water is dispersed in the form of droplets.

Prevention of hydrate formation

Several methods are applied for the prevention of hydrate formation in pipelines and these include controlling temperature and pressure, removing water, clearing the fluid, and using chemical inhibitors such as methanol or monoethylene glycol, and low-dosage hydrate inhibitors, which are used because of the conditions of the environment and also for economic reasons (Shi *et al.*, 2018). By the use of these methods, there is a change in the operating conditions of the process so as to keep the temperature and pressure outside the hydrate formation condition. In addition, the removal of water from the gas stream in the transmission lines and the addition of chemical compounds also help to maintain the temperature and operating pressure outside

the hydrate formation range (Afif *et al.*, 2016).

In addition to the primary causes, Ding *et al.*, (2016), have indicated that there are also secondary factors that favor hydrate formation and these include high fluid velocities, agitation, pressure, pulsations or any source of fluid turbulence, and the presence of CO_2 and H_2S.

Hydrate Dissociation

Hydrates dissociate when the pressure-temperature conditions are outside the hydrates stability region. Hydrate dissociation produces free gas, gas-saturated water, and water vapor saturated gas. Figure 2 shows the Pressure-Temperature (P-T) hydrate dissociation graph. Hydrate dissociation starts when the P-T state reaches the equilibrium boundary (point B in Figure 2). The P-T state remains on the phase boundary during heating under restricted volume expansion until all hydrate dissociates (region B to C in Figure 2). The increase in temperature within the stability zone (A to B in Figure 2) causes an initial breakdown of the hydrate structure due to the increased gas solubility in the surrounding pore water.

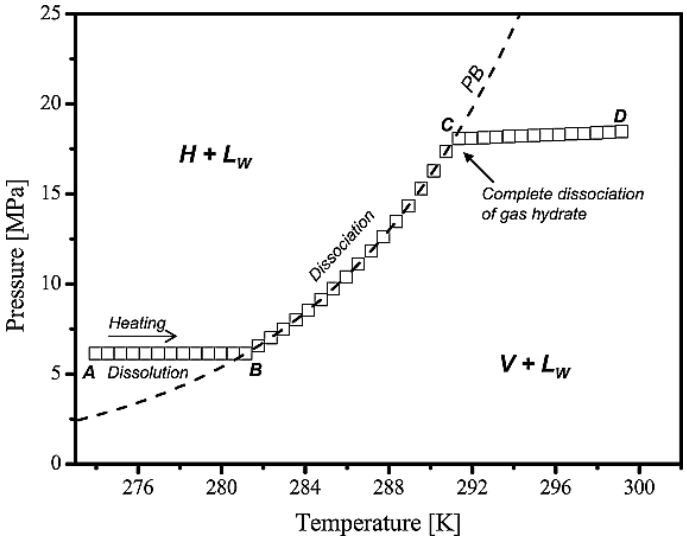

Figure 2: Hydrate Dissociation (Mustapha, 2018)

Additional increase in temperature under limited or constrained volume expansion conditions lead to increase in pressure which is induced by the thermal expansion of the phases. This phenomenon is represented by region C to D in Figure 2..

Hydrate Formation and Dissociation curves

Hydrate formation and dissociation curves were predicted with the use of thermodynamic software based on the composition of the hydrocarbon and aqueous phases in the system and are used to define pressure/temperature relationships in which hydrates form and dissociate. They define the temperature and pressure envelope in which the entire subsea hydrocarbons system must operate under steady-state and transient conditions so as to avoid formation of hydrates (Seyyedbagheri and Mirzayi, 2016). For example, with respect to natural gas, Figure 3 shows the stability of hydrates as a function of pressure and temperature. The region in which hydrates do not form is to the right of the dissociation curve and by operating in this region, there is the possibility to avoid hydrate blockages. The region to the left of the hydrate formation curve is that where hydrates are thermodynamically stable and have the potential to form (Chen *et al.*, 2018). The stability of hydrates increases with increasing pressure and decreasing temperature.

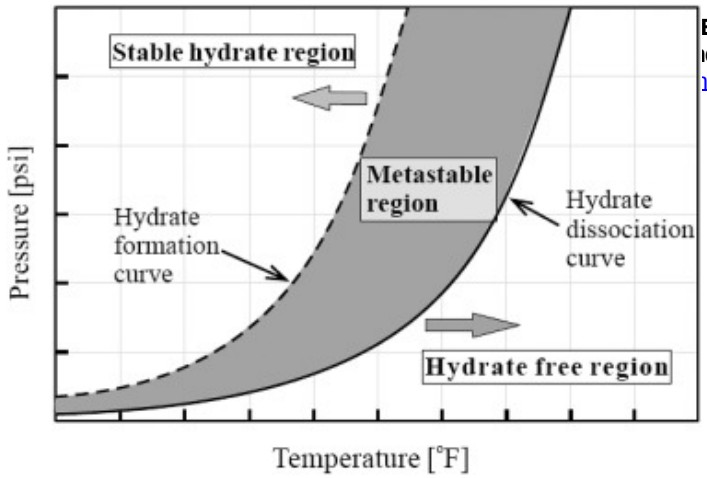

Figure 3: Hydrate Formation and Dissociation Regions (Nik, 2021)

Also to be defined is the subcooling temperature which is defined as the difference between hydrate stability temperature and the actual operating temperature at the same pressure (Nik, 2021). In this regard, the subcooling of a system without hydrate formation leads to an area between the hydrate formation temperature and the hydrate dissociation temperature, which is referred to as the metastable region, and in this region hydrates are not stable. It is to be noted that hydrates may not form for hours, days, or even at all, if a hydrocarbon system containing water is at temperature and pressure conditions close to the hydrate dissociation curve.

The hydrate dissociation curve may also be shifted toward lower temperatures by adding a hydrate inhibitor such as methanol, glycols, or sodium chloride. Hammer schmidt suggested a simple formula to estimate the temperature shift of the hydrate formation curve. This is given as follows:

$$\Delta T = KW/M(100-W),$$

where ΔT is the temperature shift (°C);

K is a constant that depends on the inhibitor. For example, K values for some inhibitors are as follows: MeOH = 2335 for MEG = 2700 and for TEG, 5400.

W is the concentration of the inhibitor in weight percent in the aqueous phase, and
M is the ratio of the molecular weight of the inhibitor to the molecular weight of water.

Hydrate Formation and Subcooling temperature

Figure 4 shows the relationship between hydrate formation time and the subcooling temperature. As the subcooling temperature increases, the hydrate formation time decreases exponentially. In general, subcooling higher than 5°F will cause hydrate formation at the hydrocarbon/water interface in flowlines. During oil production operations for example, temperatures are usually above the hydrate formation temperature, even when the system pressure is very high up to 5000 to 10,000 psi.

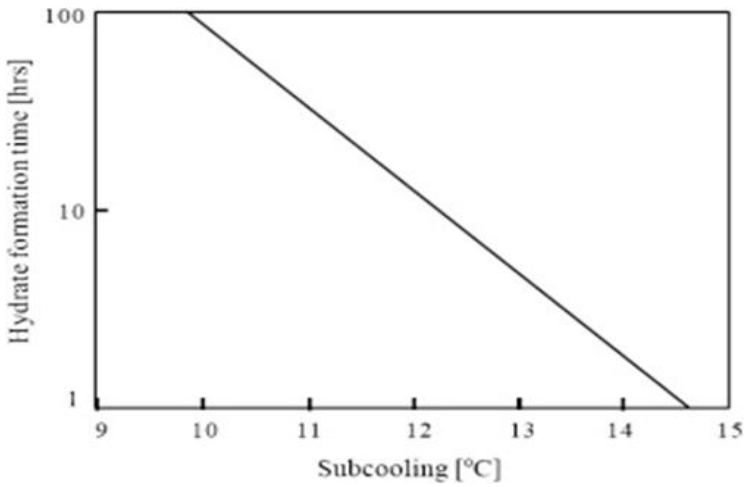

Figure 4: Variation of Hydrate Formation Time with Subcooling (Nik, 2021)

Hydrate formation Correlations

A correlation for gas hydrate formation was proposed by Hammer Schmidt as follows:

$$T_{(F)} = 8.9P_{psi}^{0.28}$$

where T and P are the temperature and pressure of hydrate formation,

respectively. This Equation does not however take into consideration the effect of the specific gravity of the gas.

Pressure explicit hydrate correlations have also been proposed. Makogon presented a P-explicit correlation which was later developed by Elgibaly and Elkamel (1998). A modified form of the Makogon correlation is presented as follows:

$$\log P_{(MPa)} = \beta + 0.0497(T_{oC} + kT_{oC}^2) - 1$$

where:

$\beta = 2.681 - 3.811\gamma + 1.679\gamma^2$

$k = -0.006 + 0.011\gamma + 0.011\gamma^2$

γ=gas specific gravity

$\gamma = MW_{Gas} / MW_{Air}$

In 1986, Berg proposed two T-explicit correlations for $0.55 \leq \gamma < 0.58$ and $0.58 \leq \gamma < 1$ with 11 and 10 adjustable parameters, respectively. To provide more precise estimations of Hydrate Formation Temperature, in 1987, Kobayashi recommended a complicated T-explicit correlation made of 15 adjustable parameters (Smith and Barifcani, 2018).

In order to properly model the formation of hydrate, the stage at which there is an adequate mass transfer for both the gas and water phases is noted, and the following expression is applicable (Bjørn, 2021).

$$M_{hydrate} = (\rho_{water}\nabla_{water}) + (\rho_{gas}\nabla_{gas})$$

where

$M_{hydrate}$ is the Mass of gas hydrate

ρ_{water} is the density of water

∇_{water} is the volume fraction of water

ρ_{gas} is the density of gas

∇_{gas} is the volume fraction of gas

MODEL EQUATIONS

For the prediction of hydrate formation phenomena, equations of continuity, momentum, and energy balances are solved simultaneously.

Following Newton's second law, mathematically this expression holds:

$$f = m.a$$

Where *f* is force, *m* is mass and *a* is acceleration

From the conservation principle,

$$\sum \vec{F} = m.\frac{\Delta \vec{V}}{\Delta t} = m.\frac{\partial(\vec{V})}{\partial t} = m.\left(\frac{\partial \vec{V}}{\partial x}\frac{\partial x}{\partial t} + \frac{\partial \vec{V}}{\partial y}\frac{\partial y}{\partial t} + \frac{\partial \vec{V}}{\partial z}\frac{\partial z}{\partial t}\right) \quad (1)$$

By convention, momentum change is thus,

$$\int m.\left(\left[\frac{\partial \vec{V}}{\partial x}dt\right] + \left[\frac{\partial \vec{V}}{\partial x}dx\right]\vec{\imath} + \left[\frac{\partial \vec{V}}{\partial y}dy\right]\vec{\jmath} + \left[\frac{\partial \vec{V}}{\partial z}dz\right]\vec{k}\right) \quad (2)$$

Momentum change with time,

$$\frac{\partial}{\partial t}\left[\int m.\left(\left[\frac{\partial \vec{V}}{\partial x}dt\right] + \left[\frac{\partial \vec{V}}{\partial x}dx\right]\vec{\imath} + \left[\frac{\partial \vec{V}}{\partial y}dy\right]\vec{\jmath} + \left[\frac{\partial \vec{V}}{\partial z}dz\right]\vec{k}\right)\right] \quad (3)$$

The conventional terms can be rewritten for an infinitesimal volume dx, dy, dz,

$$\rho\left(\left[\frac{\partial \vec{V}}{\partial t}\right] + \left[\frac{\partial \vec{V}}{\partial x}\frac{\partial x}{\partial t}\right]\vec{\imath} + \left[\frac{\partial \vec{V}}{\partial y}\frac{\partial y}{\partial t}\right]\vec{\jmath} + \left[\frac{\partial \vec{V}}{\partial z}\frac{\partial z}{\partial t}\right]\vec{k}\right)dxdydz \quad (4)$$

The velocity component in the x, y, z coordinates are represented by $\frac{\partial x}{\partial t}, \frac{\partial y}{\partial t} and \frac{\partial z}{\partial t}$ respectively.

The momentum change per unit volume is thus;

$$\rho\left(\left[\frac{\partial \vec{V}}{\partial t}\right] + \left[\frac{\partial \vec{V}}{\partial x}Vx\right]\vec{\imath} + \left[\frac{\partial \vec{V}}{\partial y}Vy\right]\vec{\jmath} + \left[\frac{\partial \vec{V}}{\partial z}Vz\right]\vec{k}\right) \quad (5)$$

Continuity equation

It states that the rate at which mass enters a system is equal to the rate at which mass leaves the system plus the accumulation of mass within the system. The continuity equation is given below;

$$\frac{\partial}{\partial_t}(\varrho) + \nabla(\varrho.v) = 0 \quad (6)$$

Where ρ is the density,
t is the time,
∇ is the volume fraction,
v is flow velocity.

Momentum equations

It states that the rate of change in linear momentum of a volume moving with a fluid is equal to the surface forces and the body forces acting on a fluid. The left side of the equation describes acceleration and is composed of time-dependent and convective components. The right side of the equation is in

the effect of a summation of volume fraction of viscosity, velocity, and body forces.
From equation 3.6,

$$\underbrace{\frac{\partial}{\partial_t}(\rho v)}_{Change\ in\ velocity\ with\ time} + \underbrace{\nabla(\rho v \mu)}_{\text{Convective term}} = \underbrace{-\nabla P}_{Pressure\ gradient} + \underbrace{\rho g}_{Body\ force\ term} + \underbrace{\mu \nabla^2 v}_{Diffusion\ term}$$

(7)
Where μ is the volume fraction fluid viscosity
∇ is the volume fraction
ρ is the density
g is the body acceleration
v is the flow velocity
P is the fluid pressure

Energy balance equation
It is an expression of the first law of thermodynamics which states that energy into a body is equal to the energy out of the body. The energy equation is given as;

$$\underbrace{\frac{\partial}{\partial t}(\rho E)}_{energy\ change\ with\ time} + \underbrace{\nabla.\big(v(\rho E + p)\big)}_{\text{convective term}} = \underbrace{-\nabla.q}_{diffusion\ term} + \underbrace{S_E}_{energy\ source} + \underbrace{\nabla.(\tau.v) + \rho g.v}_{\text{pressure work}}$$

(8)

Where E is the energy,
∇ is the volume fraction,
v is the fluid velocity,
p is pressure,
g is the body force,
ρ is the density,
q is the heat flux,
τ is the shear stress,
S_E is the energy source.

Hydrate formation model equation
The composition of natural gas considered at the inlet condition includes the molar concentration used as input to acquire the data. From the data, the pressure-temperature equilibrium curve for hydrate formation is then obtained. However, from the best fit obtained in the graph, the intercept and the slope form the basis for

the hydrate formation threshold temperature.

$T = 8.5274 \times \ln P + 270.86$ (9)

Where P is pressure in MPa
T is the temperature in Kelvin
The saturated temperature according to the partial pressure of the vapor is thus;

$$T^{sat} = 16.335 * \ln P + 167.08 \quad (10)$$

Hydrate dissociation model equation

The hydrate dissociation rate equation model considering the dissociation kinetics is thus represented below (Jarrar *et al.*, 2020).

$$-\frac{d_{nH}}{dt} k_d A_s (f_e - f)$$

where,
$\frac{d_{nH}}{dt}$ is hydrate molar dissociation rate,
k_d represents the hydrate dissociation constant,
A_S is the surface area of hydrate,
f_e is the hydrate fugacity at equilibrium pressure and temperature conditions,
f is the fugacity of gas in the bulk gas phase.
The constant for hydrate dissociation rate is represented by the Arrhenius equation:

$$k_d = k_d^0 e^{-\frac{\Delta E}{RT}}$$

Where k_d^0 is intrinsic dissociation rate constant
R is the gas rate constant
ΔE is the activation energy
T is the absolute temperature
It is noted that the dissociation rate constant is independent of temperature, hydrate surface area, and pressure.

METHODOLOGY

Simulations were carried out using the Schlumberger OLGA software which gave results consisting of trend and profile plots for hydrate formation and also in the case where mono ethylene glycol (MEG) was used for inhibiting hydrate formation. It was assumed that the material used for the transport of the fluid is steel with a conductivity of 50W/m-k, a pipeline length of

70000m, and roughness of 0.00005m. A simulation was carried out with an assumption of incompressible flow condition of the fluid on the CFD simscale software. The flow in the pipeline was considered to be turbulent and isothermal, with no interphase mass transfer occurring. The boundary conditions were inlet pressure of 500Pa and outlet pressure of 300Pa and a no-slip condition.

Simscale software; The theoretical framework of the simscale simulation was based on Mass, energy, and momentum conservations equations**.**

A card model was designed in form of a pipe with elbows and joints. The following boundary conditions were selected: inlet fluid velocity, outlet fluid velocity, inlet pressure, outlet pressure. The following considerations were made:

i. The wall conditions for an incompressible fluid.

ii. The pipe was modelled under considerations of crude oil properties.

iii. A mesh was generated to allow for the simulation of the pipe model.

iv. The simulation was run for 30mins

v. Following (iv) above a plot map was developed showing the regions of high and low pressure to indicate where hydrate formation occurs.

Olga software;

i. A platform showing a workspace consisting of a component tab with flowline, battery pump, output, input was created.

ii. Properties which include material, insulation, conductivity, density were added to the model with the aid of the model browser.

iii. The flow path for the pipeline was created and configured with consideration of roughness and diameter.

iv. Boundary conditions for pressure, temperature, mass

flow rate, pipeline length were set up.

v. A parametric study showing the effect of temperature and pressure on hydrate formation with the addition of inhibitor at different flow rates was considered.

vi. Different plots showing trends and profiles under various conditions for hydrate formation were generated.

Table 2: Parameters used for the computation of the hydrate formation model

Inlet Temperature (C)	Diameter of Pipe (m)	Operating pressure (Mpa)	Volume fraction of the water feed	Feed velocity (m/s)
42	0.20	6.0	0.4	2

Table 3: Boundary conditions for Simscale simulation

Inlet fluid velocityI(m/s)	Outlet fluid velocity (m/s)	Inlet pressure (Pa)	Outlet pressure (Pa)
2.0	3.6	500	300

Table 4: Hydrate formation datasheet

Specific Gravity	No of data points	T range, K	P range, MPa
0.67	5	282 – 298	1.2 - 16
0.55	7	270 – 294	2.4 - 37
0.63	11	276 - 293	1.5 - 20
0.55	3	278 - 289	7.2 - 30
0.63	5	277 - 287	1.1 - 9
0.55	4	265 - 279	5.1 - 31
0.63	5	261 - 276	1.3 - 8.2
0.67	10	268 - 284	1.1 - 133
0.55	6	263 - 272	10 - 31
0.63	13	259 - 275	1.9 - 36
0.67	9	265 - 281	2.4 - 175
0.67	3	259 - 268	24 - 173
0.55	3	247 - 251	10 - 18

Table 5: Simulation options

Overall setting	Flow model	OLGA HAD
	Mass eq scheme	1ST ORDER
	Compositional model	MEG
	Debug	ON
	Drilling	OFF
	Phase	THREE
	Elastic walls	OFF
	Void in slug	SINTEF
	Steady-state	ON
	User-defined plug-in	OFF
	Temp. calc.	WALL
	Wax deposition	OFF
	Restart	OFF
Integration	Simulation start time	0 s
	Simulation stop time	1 h
	Minimum time step	0.01 s
	Maximum time step	5 s

Table 6: Insulation materials and parameters

Label	**Density**	**Conductivity Capacity**	**Heat**
STEEL	7850 kg/m3	50 W/m-K	500 J/kg-C
INSULATION	1000 kg/m3	0.135 W/m-K	1500 J/kg-K
FBE Coating	1300 kg/m3	0.3 W/m-K	1410 J/kg-C

Table 7: Boundary conditions for Olga software

Label	Type	Pressure	Temperature
ONSHORE-PLANT	PRESSURE	80 bar	6 ^{o}C
TEMPLATE	CLOSED		

RESULTS AND DISCUSSION

The flow path plot is shown in Figure 6. The reddish spots on the profile plots as shown in Figure 7, indicate points of high pressure and possible formation of hydrates.

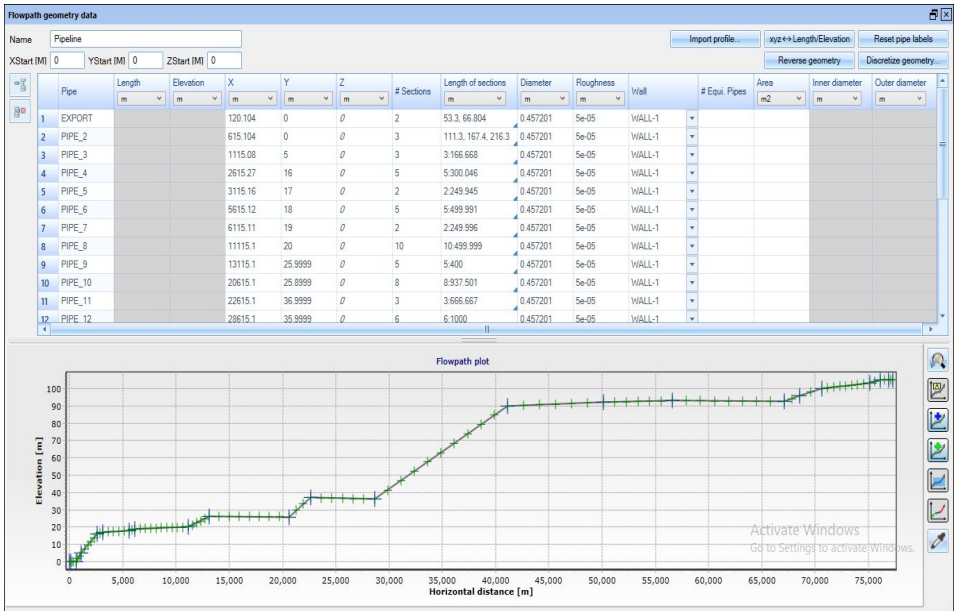

Figure 6: Flow path Plot

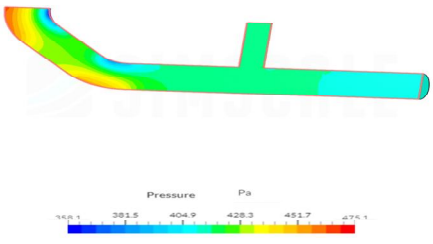

Figure 7: Simulation of incompressible flow through the pipeline

Effects of fluid flow and the pipeline conditions on the hydrate formation

A decrease in temperature shows hydrates formation while an increase in temperature shows hydrates dissociation. Figure 8 shows hydrates form and dissociates times in the pipe as fluid flows through. At 2000s, there is maximum formation of hydrates. As the time further increase hydrates dissociate due to increase in temperature.

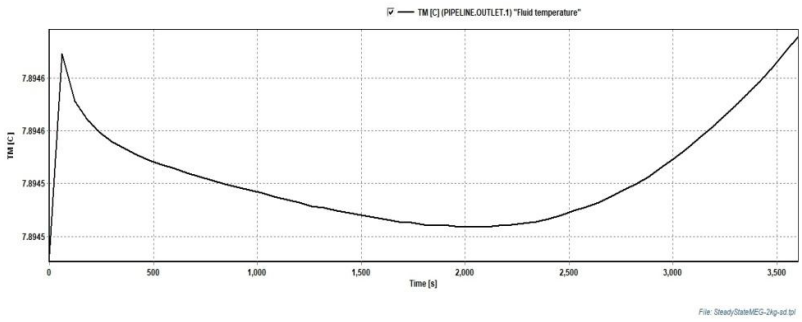

Figure 8: Trend plot simulation result for hydrate formation

From Figure 9, it is seen that temperature decreases as the pipe length increases. Therefore, hydrates form as fluid flows through the pipe at increasing length and decreasing temperature.

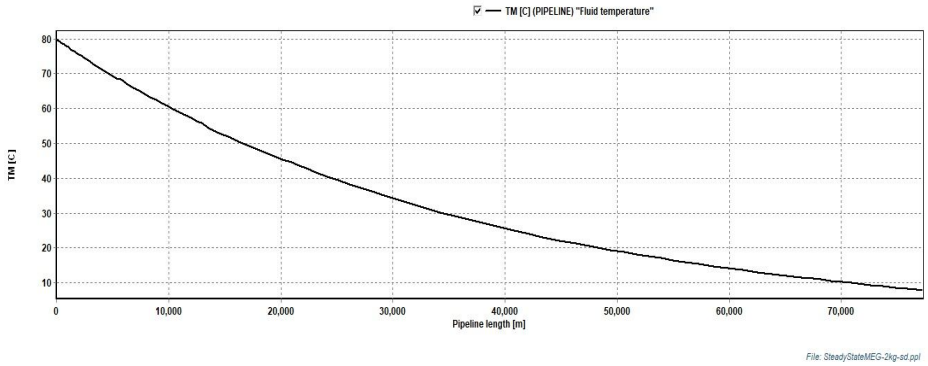

Figure 9: Profile plot simulation result for hydrate formation

From Figure 10, pressure decreases as the pipe length increases. Therefore, hydrates dissociate due to reduced pressure at increased pipeline length.

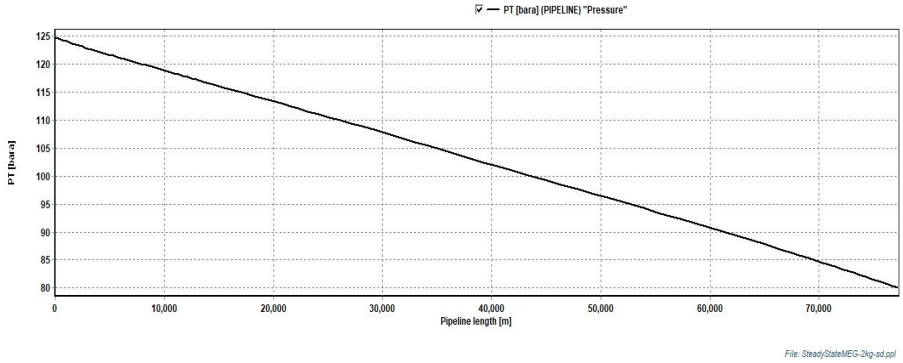

Figure 10: Profile plot simulation result for hydrate dissociation

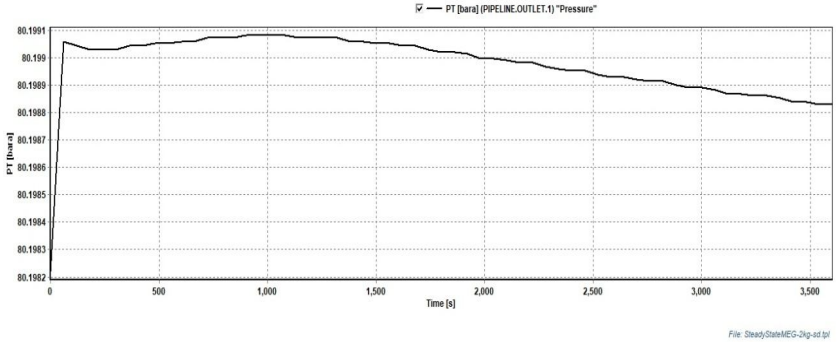

Figure 11: Trend plot simulation result for hydrate formation

From Figure 11, it is seen that after 1000s, there is a maximum formation of hydrates. As the pressure reduces over time, hydrates dissociate along the pipeline. Simulations were carried out with the introduction of inhibitors. The cases indicate the introduction of different mass flow rates of MEG inhibitor.

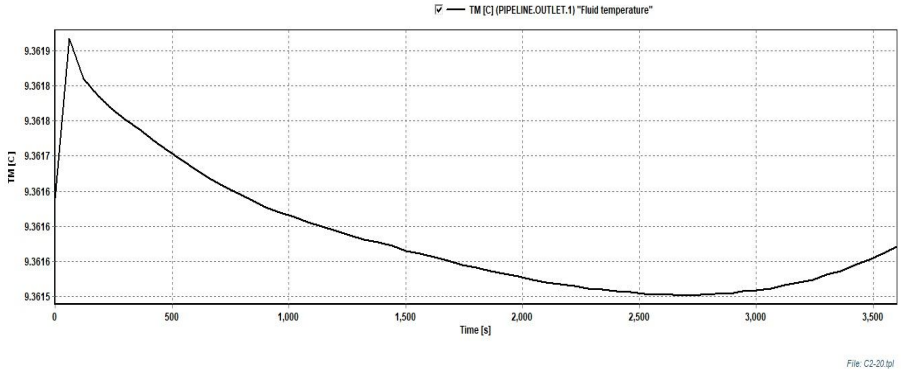

Figure 12: Effect of inhibitor at 20kg/s mass flow rate on hydrate dissociation in pipeline

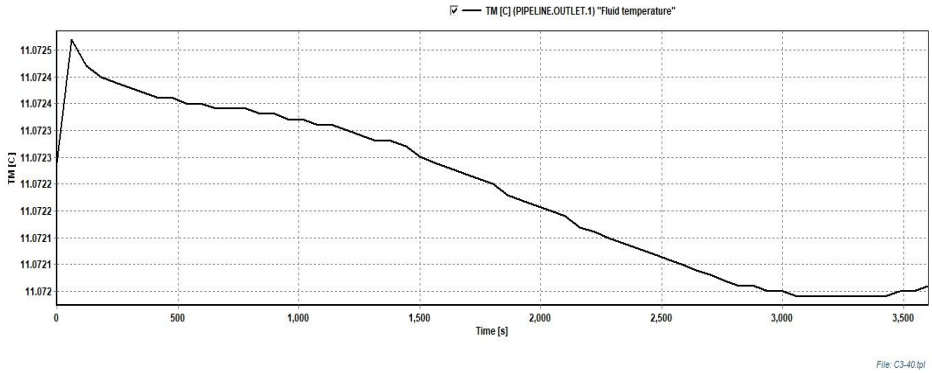

Figure 13: Effect of inhibitor at 40kg/s mass flow rate on hydrate dissociation in pipeline

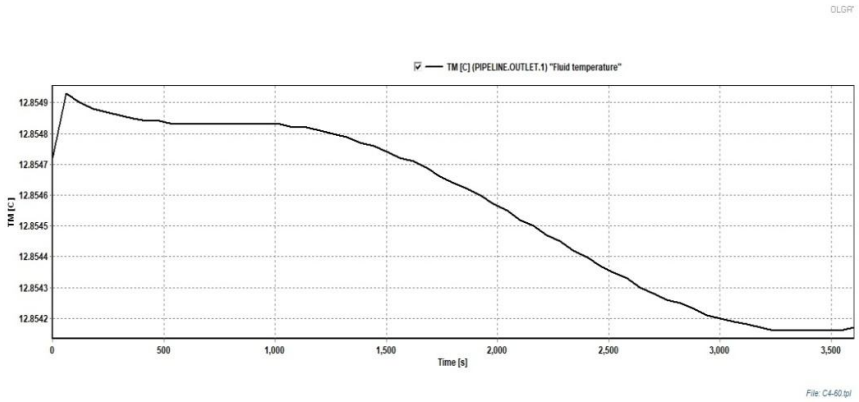

Figure 14: Effect of inhibitor at 80kg/s mass flow rate on hydrate dissociation in pipeline

Figures 12, 13 and 14, show the effect of inhibitor at different mass flow rates with time. A gradual increase in temperature was observed. The introduction of MEG reduces and possibly eliminates the hydrate formation as observed in the profiles.

CONCLUSION

In this study, CFD software was employed to simulate the hydrate formation along a pipeline. The pipeline simulation was obtained employing the model's boundary conditions. The hydrate formation temperatures were compared to find the probability of hydrate formation along the pipeline. The effects of parameters such as initial temperature, mass flow rate, pipeline length, and pressure were considered as possible hydrate formation agents. The results indicate that the inlet temperatures were high, so the possibility of hydrate formation at the entrance of the pipeline was ruled out. In addition, as a result of increase in pressure and decrease in temperature as the fluid travels along the pipeline, hydrate formation is possible. Furthermore, an increase in the inhibitor flow rate decreases the chances of hydrate formation.

REFERENCES

Afif, A., Majid, A., Chaudhari, P., Koh, C. A. and Sum, A. K. (2016) 'Gas Hydrate Formation & Interactions for Water Continuous & Partially Gas Hydrate Formation & Interactions for Water Continuous & Partially', (April 2020). DOI: 10.4043/27277-MS.

Bjørn (2021) 'Kinetics of hydrate formation , dissociation and reformation', (6359). doi: 10.1016/j.ctta.2021.100004 .

Chen, Y., Shi, B., Liu, Y. and Song, S. (2018) 'Progress of influence mechanism of kinetic hydrate inhibitors', (December 2019).

Ding, L., Ding, L., Shi, B., Lv, X., Liu, Y., Wu, H., Wang, W. and Gong, J. (2016) 'Investigation of natural gas hydrate slurry flow properties and flow patterns using a high-pressure flow loop, *Chemical Engineering Science*. Elsevier, 146(March), pp. 199–206. DOI: 10.1016/j.ces.2016.02.040.

Elgibaly A.A. and Elkamel A.M.(1998). A New Correlational for Predicting Hydrate Formation Conditions for Various Gas Mixtures and Inhibitor Fluid Phase Equilibra, 152, 23-42

Gong, J. and Lv, X. (2013) 'A study of hydrate plug formation in a subsea natural gas pipeline using D QRYHO KLJK SUHVVXUH ÀRZ ORRS', (March). DOI: 10.1007/s12182-013-0255-8.

Jai, S., Sahith, K. and Pedapati, S. R. (2020) 'applied sciences Investigation on Gas Hydrates Formation and Dissociation in Multiphase Gas Dominant Transmission Pipelines'.

Jarrar, Z. A., Alshibli, K. A.,

Al-raoush, R. I. and Jung, J. (2020) '3D measurements of hydrate surface area during hydrate dissociation in porous media using dynamic 3D imaging', *Fuel*. Elsevier, 265(October 2019), p. 116978. DOI: 10.1016/j.fuel.2019.116978.

Liu, Z. (2017) 'Study of Hydrate Deposition and Sloughing OF GAS-Dominated Pipelines using Numerical and Analytical Models'. PhD Thesisis Colorado School of Mine.

Majlesara, M., Salmanzadeh, M. and Ahmadi, G. (2013) 'A model for particles deposition in turbulent inclined channels', *Journal of Aerosol Science*. Elsevier, 64(October), pp. 37–47. DOI: 10.1016/j.jaerosci.2013.06.001.

Mamasani, A., Azari, A., Izadpanah, A. A. and Jamali, M. (2019) 'Prediction of hydrate formation in Ilam gas refinery pipeline using computational fluid dynamic', 6(1), pp. 63–81.

Merey, Ş., and Longinos, S. N. (2018) 'Numerical simulations of gas production from Class 1 hydrate and Class 3 hydrate in the Nile Delta of the Mediterranean Sea', *Journal of Natural Gas Science and Engineering*. Elsevier BV, (March 2021). DOI: 10.1016/j.jngse.2018.01.001.

Naseer, M. and Brandst, W. (2018) 'Hydrate formation in natural gas pipelines', 70, pp. 261–270. DOI: 10.2495/MPF110221.

Nik, S. (2021) 'Potential environmental challenges for gas hydrates', (March).

Seyyedbagheri, H. and Mirzayi, B. (2016) 'CFD

Modeling of High Inertia Asphaltene Aggregates Deposition in 3D Turbulent Oil Production Wells CFD modeling of high inertia asphaltene aggregates deposition in 3D turbulent oil production wells', *Journal of Petroleum Science and Engineering*. Elsevier, 150(January 2018), pp. 257–264. DOI: 10.1016/j.petrol.2016.12.017.

Seyyedbagheri, H. and Mirzayi, B. (2017) 'Eulerian Model To Predict Asphaltene Deposition Process in Turbulent Oil Eulerian Model To Predict Asphaltene Deposition Process in Turbulent Oil Transport Pipelines', (August 2020). DOI: 10.1021/acs.energyfuels.7b01273.

Shi, B., Chai, S., Wang, L., Lv, X., Liu, H., Wu, H. and Wang, W. (2016) 'Viscosity investigation of natural gas hydrate slurries with anti-agglomerates additives Viscosity investigation of natural gas hydrate slurries with anti-agglomerates additives', (July). DOI: 10.1016/j.fuel.2016.07.113.

Shi, B., Song, S., Lv, X., Li, W., Wang, Y., Ding, L. and Liu, Y. (2018) 'Investigation on natural gas hydrate dissociation from a slurry to a water-in-oil emulsion in a high-pressure flow loop Investigation on natural gas hydrate dissociation from a slurry to a water-in-oil emulsion in a high-pressure flow loop', *Fuel*. Elsevier, 233(December), pp. 743–758. DOI: 10.1016/j.fuel.2018.06.054.

Smith, C. and Barifcani, A. (2018) 'Gas Hydrate Formation And Dissociation Numerical Modelling with Nitrogen and Carbon Dioxide'.

Yao, S., Li, Y., Wang, W., Song, G., Shi, Z., Wang,

X. and Liu, S. (2019) 'Investigation of hydrate slurry flow behaviors in deep-sea pipes with different inclination angles, 48..